Atmos. Chem. Phys., 17, 3891–3903, 2017
www.atmos-chem-phys.net/17/3891/2017/
doi:10.5194/acp-17-3891-2017

Atmospheric Chemistry and Physics
Open Access
EGU

Lower tropospheric distributions of O_3 and aerosol over Raoyang, a rural site in the North China Plain

Rui Wang[1], Xiaobin Xu[1], Shihui Jia[1,a], Ruisheng Ma[2], Liang Ran[3], Zhaoze Deng[3], Weili Lin[4], Ying Wang[1], and Zhiqiang Ma[5]

[1]State Key Laboratory of Severe Weather & Key Laboratory for Atmospheric Chemistry of China Meteorological Administration, Chinese Academy of Meteorological Sciences, Beijing, China
[2]Guangxi Meteorological Disaster Mitigation Institute, Nanning, Guangxi, China
[3]Key Laboratory of Middle Atmosphere and Global Environment Observation, Institute of Atmospheric Physics, Chinese Academy of Sciences, Beijing, China
[4]Meteorological Observation Center, China Meteorological Administration, Beijing, China
[5]Institute of Urban Meteorology, China Meteorological Administration, Beijing, China
[a]now at: School of Environment and Energy, South China University of Technology, Guangzhou, Guangdong, China

Correspondence to: Xiaobin Xu (xuxb@camscma.cn)

Received: 25 October 2016 – Discussion started: 9 November 2016
Revised: 1 March 2017 – Accepted: 6 March 2017 – Published: 21 March 2017

Abstract. The North China Plain (NCP) has become one of the most polluted regions in China, with the rapidly increasing economic growth in the past decades. High concentrations of ambient O_3 and aerosol have been observed at urban as well as rural sites in the NCP. Most of the in situ observations of air pollutants have been conducted near the ground so that current knowledge about the vertical distributions of tropospheric O_3 and aerosol over the NCP region is still limited. In this study, vertical profiles of O_3 and size-resolved aerosol concentrations below 2.5 km were measured in summer 2014 over a rural site in the NCP, using an unmanned aerial vehicle (UAV) equipped with miniature analyzers. In addition, vertical profiles of aerosol scattering property in the lower troposphere and vertical profiles of O_3 below 1 km were also observed at the site using a lidar and tethered balloon, respectively. The depths of the mixed layer and residual layer were determined according to the vertical gradients of lidar particle extinction and aerosol number concentration. Average O_3 and size-resolved aerosol number concentration in both the mixed and residual layer were obtained from the data observed in seven UAV flights. The results show that during most of the flights the O_3 levels above the top of mixed layer were higher than those below. Such a positive gradient in the vertical distribution of O_3 makes the residual layer an important source of O_3 in the mixed layer, particularly during the morning when the top of mixed layer is rapidly elevated. In contrast to O_3, aerosol number concentration was normally higher in the mixed layer than in the residual layer, particularly in the early morning. Aerosol particles were overwhelmingly distributed in the size range < 1 µm, showing slight differences between the mixed and residual layers. Our measurements confirm that the lower troposphere over the rural area of the NCP is largely impacted by anthropogenic pollutants locally emitted or transported from urban areas. Compared with the historic O_3 vertical profiles over Beijing from the Measurement of Ozone and Water Vapor by Airbus In-Service Aircraft (MOZAIC), a strong increase in O_3 can be found at all heights below 2.5 km in the decade from 2004 to 2014, with the largest enhancement of about 41.6 ppb. This indicates that the lower troposphere over the northern part of the NCP has experienced rapidly worsening photochemical pollution. This worsening trend in photochemical pollution deserves more attention in the future.

Published by Copernicus Publications on behalf of the European Geosciences Union.

1 Introduction

Ozone (O_3) is a key trace gas and oxidant in the troposphere, which can generate hydroxyl radical (OH), which affects the oxidizing capacity of the atmosphere. Ground-level O_3 causes deleterious impacts on human health and vegetation (Anenberg et al., 2009; McKee, 1994; Yue and Unger, 2014; Feng et al., 2008). Meanwhile, tropospheric O_3 is an effective greenhouse gas. The fifth IPCC assessment report points out that the increase of O_3 in the troposphere has caused $+0.40$ (± 0.20) W m^{-2} of radiative forcing (Myhre et al., 2013). The vertical distribution of O_3 can influence the accumulation of O_3 in the surface layer and chemical reactions as well as a radiation budget at different altitudes. The vertical distribution of O_3 is influenced by chemical and meteorological processes and varies with time and location (Kleinman et al., 1994; Fast and Berkowitz, 1996; Lin et al., 2007; Ma et al., 2011). Therefore, direct measurements are needed to acquire the knowledge about the vertical distribution of O_3, which is important to understanding atmospheric chemistry and O_3 radiative forcing.

Atmospheric aerosols influence the climate by direct effect and indirect effect (Schwartz, 1996; Coakley Jr. et al., 1983; Kiehl and Briegleb, 1993; Charlson, 1997; Tegen et al., 2000). High loading of aerosols causes poor visibility and air quality. The diameters of aerosol particles span over 4 orders of magnitude, from a few nanometers to around 100 µm (Seinfeld and Pandis, 2006). Aerosol size distribution is one of the most critical factors determining light scattering property, health effects, and lifetime of aerosols. Observations of aerosol size distribution and its spatiotemporal variations have been one of the important aspects in the study of atmospheric aerosols.

The planetary boundary layer (PBL) is the lowest part of the troposphere, which is influenced to a large extent by the friction of Earth's surface and objects on it (Ahrens, 2011). The PBL is directly impacted by most of anthropogenic and natural sources of trace gases and aerosols. In the PBL, air turbulence can be so strong that it drives the rapid exchange of heat, water vapor, trace gases, and aerosols between the atmosphere and Earth's surface. The structure of the PBL is critical to the vertical diffusion and transport of air pollutants so that the changes of vertical distributions of many trace gases (such as O_3) and aerosols are closely related to the evolution of the PBL.

The diurnal evolution of the PBL usually leads to a well-developed mixed layer in the daytime (He and Mao, 2005) and a stable layer overlaid by a residual layer in the nighttime. The formation of a nocturnal stable layer may exert significant impacts on the concentrations of species in the surface layer. For example, surface O_3 is substantially removed during the night by reactions with NO and some other species, and by dry deposition, particularly in urban areas during cold seasons (Lin et al., 2011). Following the development of the mixed layer on the next day, O_3 in the residual layer can be downward mixed, making a contribution to the enhancement of ground-level O_3 and even driving photochemical processes (Aneja et al., 2000; Kleinman et al., 1994; Neu et al., 1994; Zhang and Rao, 1999). Therefore, O_3 distribution in both mixed layer and residual layer deserves attention. Similarly, chemical compositions and physical properties including size distribution of aerosols may also be impacted by the evolution of the PBL. Knowledge of this aspect is important for atmospheric chemistry and physics studies.

In recent decades, with the rapid economic development and the urbanization in China, ground-level and tropospheric O_3 and aerosol have increased significantly, especially in the North China Plain (NCP; Ding et al., 2008; Xu and Lin, 2011; Ma et al., 2016; Chen et al., 2015; Ding and Liu, 2014). So far, observational studies on O_3 and aerosol in the NCP have been mainly conducted in the surface layer. There is only limited knowledge of the vertical distributions of tropospheric O_3 and aerosol over the NCP region, gained in some sporadic observational studies (Chen et al., 2009, 2013; Ma et al., 2011; Wang et al., 2012; Zheng et al., 2005). This hinders extensive validations of atmospheric chemistry models as well as the assessment of climate effects of O_3 and aerosols over this important region.

The detection of vertical distributions of O_3 and aerosol can be made using balloon sounding, aircraft, and tethered balloons. Each of these techniques has its advantages and disadvantages. Balloon sounding is a good way of obtaining O_3 and aerosol vertical profiles below ca. 30 km, but the sondes for O_3 and aerosol are usually expensive and not reusable, not to mention the ground facilities needed for the sounding. Tethered balloons attached with O_3 and aerosol devices can be used many times for observations under stable weather conditions, but it is usually not suitable when operated above 1 km and needs manpower to run it carefully. Aircraft equipped with analyzers for O_3, other trace gases, and aerosol instruments can be used to simultaneously obtain distributions of these species along the flight tracks, but such observations are normally expensive and need the strong logistic support of an airport.

Typically, most aircraft measurements are made using manned aircrafts. However, unmanned aerial vehicles (UAVs) can also be used as research platforms. In the last decade, UAVs have been successfully used in the fields of atmospheric science and environmental monitoring in order to understand the three-dimensional distribution of atmospheric species (Altstädter et al., 2015; Illingworth et al., 2014; Watai et al., 2006; Rauneker and Lischeid, 2012; Gao et al., 2016). In comparison with manned aircrafts, UAVs have a few advantages, such as no need for an airport, lower costs, higher flexibility, the possibility to investigate atmospheric parameters at small scales and low altitudes, and the potential for application in regions dangerous for manned aircraft (Altstädter et al., 2015). Above all, measurements with high spatial resolutions can be obtained using UAVs. For example,

in a city center with a diameter of approximately 2 km, a typical instrument with 1 Hz resolution would only be able to make approximately 20 measurements during an overpass of the city when a normal atmospheric research aircraft was used. In contrast, more measurements would be obtained by an UAV; therefore, the measurement uncertainty can be effectively reduced.

In this paper, we present UAV measurements of vertical distributions of O_3 and size-resolved aerosol number concentrations obtained over a site in the NCP during a field campaign. Data of surface O_3 and lidar observations of aerosol extinction from a nearby site are included in the analysis to facilitate interpretations and discussions of the measurements. To the best of our knowledge, there has been no similar published study of the region of China.

2 Experimental

2.1 Ground-based measurements

Ground-based measurements, including measurements of surface O_3 and some other reactive gases ($NO/NO_2/NO_x$, NO_y, HCHO, PAN, SO_2, CO, NH_3, etc.), tethered balloon measurements of O_3 and black carbon (BC) vertical profiles, lidar observation of aerosol vertical profiles, etc., were conducted from 7 June to 18 August 2014 at the Raoyang Meteorological Station (RMS; 115°44′, 38°14′ N; 20 m; a semirural site) in the NCP. The RMS is located in Raoyang County, an agriculture county in the middle of Heibei Province. There are no large industrial sources in Raoyang. However, some influences on the RMS site from the residence and traffic sources in the surrounding areas cannot be excluded. More details about the RMS site are given in Ran et al. (2016).

Surface O_3 was measured using a photometric O_3 analyzer (TE 49C, Thermo Electron, USA). The detection limit and precision of the O_3 analyzer are 1 and 1 ppb, respectively. The analyzer was calibrated on 17 June, 16 July, and 18 August 2014 and showed no significant drifts. Details about the calibration and maintenance are described in Lin et al. (2009). A dual-beam ozone monitor (Model-205, 2B Technologies, USA) was used for the tethered balloon observations of O_3 vertical profiles. The ozone monitor has dimensions of 9 cm × 21 cm × 29 cm and weighs only 2.3 kg. It works based on the ultraviolet (UV) absorption at 254 nm at a maximum frequency of 0.5 Hz. It measures O_3 with a precision of 1 ppb or 2 % of reading and has a limit of detection of 1 ppb. The ozone monitor was calibrated at the site using an O_3 calibrator (TE 49i-PS, Thermo Electron, USA).

Vertical profiles of aerosol were observed using a lidar (Leosphere, France). The lidar principle is based on the scattering phenomenon of light. A laser pulse is sent into the atmosphere and scattered by the target molecules or particles (clouds, dust, soot particles, etc.). The backscattered light is collected by an optical system and its intensity is measured by a photo-detector, converted into an electronics signal, and stored onto a computer. The wavelength of the laser sent is 355 nm. The vertical resolution of the lidar measurement is 15 m and data below 200 m are discarded (EZ aerosol and cloud lidar ALS300 & ALS450 user manual).

2.2 Flight information

An UAV platform was used for the vertical profile measurements. The body of the UAV is made of glass fiber reinforced plastics, with a wingspan of 3.2 m. The UAV is battery-powered so that there is no contaminant from the engine exhaust of the UAV. The cruising speed and maximum cruising altitude of the UAV are 25 m s^{-1} and 5.5 km, respectively. As we were more interested in the vertical distributions of O_3 and aerosol in the lower troposphere, the UAV was programmed to fly below 3 km over an area within 5 km in diameter.

A miniature ozone monitor, personal ozone monitor (POM; 2B Technologies, USA) and handheld optical particle counter (OPC; Handheld 2016 or 3016, Lighthouse, USA) were installed in the small cabinet of the UAV to measure the O_3 and aerosol number concentrations on the flight. The POM has dimensions of 10.2 cm × 7.6 cm × 3.8 cm and weighs only 0.34 kg. It works based on the UV absorption at 254 nm at a maximum frequency of 0.1 Hz. It measures O_3 with a precision of 2 ppb or 2 % and has a limit of detection of 4 ppb, well below the normal O_3 level over the Raoyang site. The POM was calibrated in the factory against a National Institute of Standards and Technology (NIST)-traceable standard instrument and compared at the site with the TE 49i-PS O_3 calibrator. The handheld OPC has dimensions of 22.23 cm × 12.7 cm × 6.35 cm and weighs about 1 kg. The Handheld 2016 counts aerosol numbers in the size bins 0.2–0.3, 0.3–0.5, 0.5–0.7, 0.7–1.0, 1.0–2.0, and > 2 µm, while the Handheld 3016 (used only in the flight during 05:53–06:18 local time (LT) of 31 July) records aerosol numbers in the size bins 0.3–0.5, 0.5–1.0, 1.0–3.0, 3.0–5.0, 5.0–10.0, and > 10 µm in differential or accumulation method. The OPC devices were set to collect data at 1 Hz. An isokinetic tube was mounted on the nose of the UAV to introduce ambient air into the OPC. In addition, a temperature–humidity sensor was attached to the OPC so that the sampling flow rate was converted to standard condition. Both OPC devices were calibrated against a NIST-traceable source. More details are given in the Supplement (Sect. S1).

Limited mainly by the availability of airspace, only seven successful UAV measurements were conducted several kilometers west of the RMS during the observation period. More detailed flight information is summarized in Table 1.

Table 1. The ascent and descent flight time (local time, LT) and the maximum height.

Flight	Date	Ascent period	H_{max} (m)	Descent period
1	29 June	10:18–10:36	1316	10:36–10:47
2	29 June	17:58–18:24	2498	18:24–18:38
3	1 July	06:34–06:55	2021	06:55–07:07
4	29 July	07:35–07:51	2430	07:51–08:04
5	31 July	05:53–06:18	2468	06:18–06:33
6	31 July	17:26–17:44	2676	17:44–18:02
7	2 August	15:17–15:29	2410	15:29–15:45

3 Results and discussion

3.1 Vertical profiles of O_3, aerosol number concentration and extinction

The vertical profiles of O_3 were acquired during seven UAV flights as listed in Table 1, while aerosol number concentrations in six size bins were observed during five of the seven flights (flights 1–5). The observed aerosols particles were predominately distributed in the accumulation mode since it is not possible to count the aerosol numbers in the Atkin mode using the handheld OPC. Figure 1 shows the vertical profiles of O_3 and aerosol number concentration observed during all flights. To study how the evolution of PBL influences O_3 and aerosol concentration at different altitudes, the vertical profiles in Fig. 1 are grouped in early morning (05:40–08:00 LT), late morning (10:00–12:00 LT), and afternoon (15:00–19:00 LT) periods and shown in Fig. 1a, b, and c, respectively. In addition, average particle extinction vertical profiles simultaneously obtained by the lidar are presented, with data points less than or equal to zero being excluded. All the vertical profiles shown in Fig. 1 include averages over 50 m vertical layers, regardless of the spatial resolutions of actual observations. Although the site over which the flights were conducted is several kilometers away from the RMS, both sites were influenced by the same synoptic system. Therefore, the results (Fig. 1) from both sites should be comparable within the observation uncertainties. In the early morning of 29 July 2014, particle extinction of more than 3000 Mm^{-1} was observed at around 1600 m (Fig. 1a3), indicating the presence of cloud there (Huang et al., 2011).

It is noteworthy in Fig. 1 that aerosol number concentrations during late morning of 29 June (flight 1) and early morning of 1 July (flight 3) and the O_3 mixing ratio during late morning of 29 June (flight 1) were significantly lower than those during other flights, and their vertical profiles were slightly different from others. This indicates that some factors might have impacted the levels and vertical profiles of O_3 and aerosol. To understand those phenomena, we display the airflow fields at 1000 and 850 hPa over the area surrounding RMS in Fig. S2 in the Supplement, and 48 h backward trajectories of air parcels arriving at 100, 500, 1000, 1500, and 2000 m over RMS in Fig. S3 in the Supplement for 08:00 LT

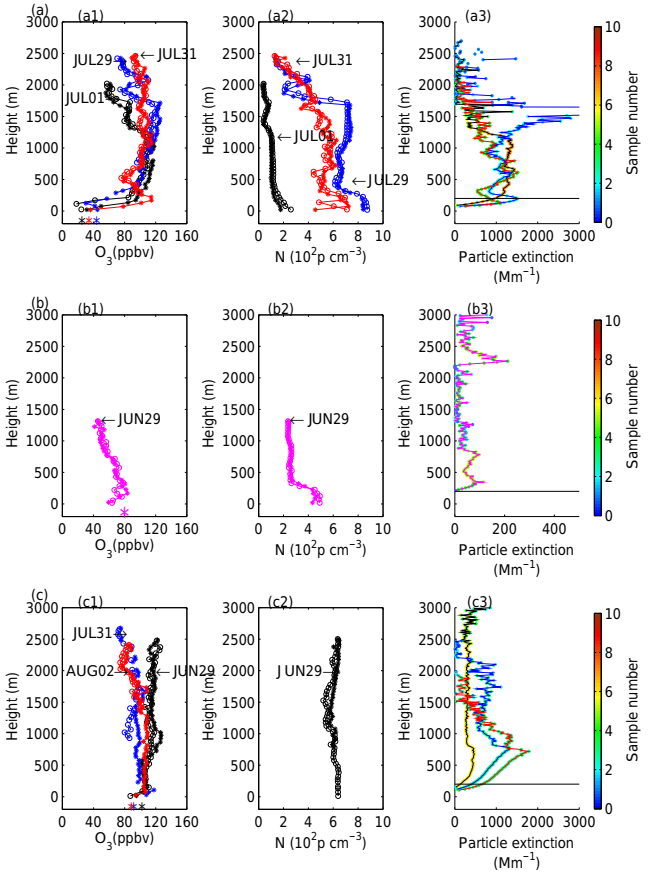

Figure 1. Vertical profiles of O_3 **(a1, b1, c1)**, aerosol number concentration **(a2, b2, c2)** and particle extinction **(a3, b3, c3)** obtained in **(a)** early morning, **(b)** late morning, and **(c)** the afternoon, respectively. The O_3 and aerosol vertical profiles obtained during the ascent and descent of the UAV are indicated with circles and asterisks, respectively. Ground-level O_3 mixing ratios during the flights are also shown together with the O_3 vertical profiles (bigger asterisks with a negative offset in altitude). The color scales attached to particle extinction graphs **(c1, c2, c3)** show the sample numbers of individual particle extinctions, from which the averages of particle extinctions were calculated. The black lines indicate the altitude of 200 m above ground, under which the particle extinction data should not be used.

of 29 June, 1 July, 29 July, and 31 July 2014, calculated using the Hybrid Single-Particle Lagrangian Integrated Trajectory model (Draxler and Rolph, 2003).

Figure S2a and b indicate that the 1000 and 850 hPa levels on the early morning of 29 June were dominated by different air circulations. Figure S3a shows that the air parcels arriving at 100 and 500 m over RMS were from the boundary layer over the nearby areas and mainly south of the site, while those arriving at 1000 m and above originated far from the north (northern Heilongjiang) and traveled rapidly over 2000 m for most of the time. The disparate airflows in the bottom and upper layers made a large negative gradient in the vertical distributions of O_3 and aerosol number concen-

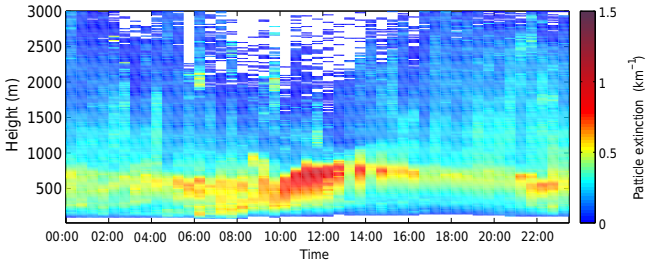

Figure 2. Average diurnal patterns of vertical distribution of particle extinction.

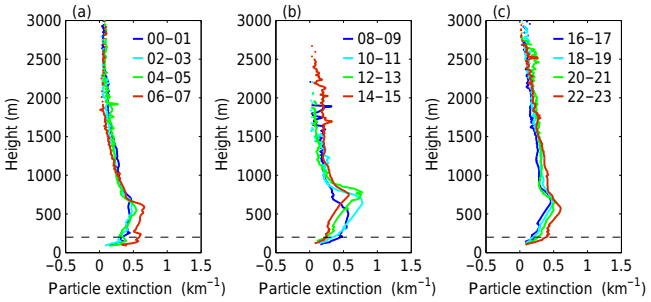

Figure 3. Vertical profiles of particle extinction averaged every 2 h for **(a)** 00:00–07:00 LT, **(b)** 08:00–15:00 LT, and **(c)** 16:00–23:00 LT.

tration during flight 1, as can be seen in the vertical profiles shown in Fig. 1b1 and b2.

In the whole layer, the aerosol number concentration in the early morning of 1 July (flight 3) was much lower than those in the other two flights (flights 4 and 5) in the early morning of 29 and 31 July (Fig. 1a2). Figure S2c and d in the Supplement show that the airflow at the 1000 and 850 hPa levels over RMS was mostly from the south-southwest. Figure S3b in the Supplement indicates that air parcels arriving at different heights over RMS originated either from the south or from the west or east bending to south. Using the Meteorological Information Comprehensive Analysis and Process System (http://www.cma.gov.cn/en2014/20150311/20160615/index.html) we found that there was rainfall within the 48 h prior to 05:00 LT of 1 July over the north, south-southwest, and the southeast of RMS. It can be inferred that in the early morning of 1 July air transported to the lower troposphere over RMS had been mixed with cleaner air during the rainy conditions so that the aerosol number concentration declined substantially. Therefore, synoptic situations are important factors influencing the concentrations of air pollutants and their vertical distributions. Another important factor is the PBL evolution, as discussed in the next section.

3.2 Determination of the mixed and residual layer depth

The PBL development can, in principle, be determined by measurement of vertical profiles of a variety of atmospheric properties, with potential temperature being the most common one (Lenschow, 1986). Vertical aerosol number concentration vertical profiles allow for the determination of the PBL, as aerosol acts as a tracer of atmospheric turbulent forces along height (Ferrero et al., 2011, 2014). One powerful way to probe the PBL is based on vertical profiles of particle extinction detected using lidar. There are several methods to explore the structure of PBL from vertical profiles of particle extinction, such as the calculation of vertical gradient of particle extinction (He and Mao, 2005; Huang et al., 2011; Hayden et al., 1994; Hoff et al., 1996; Melfi et al., 1985), wavelet analysis (Cohn et al., 1997; Brooks, 2003), and parameterization (Steyn et al., 1999). In this study, calculations of the vertical gradient of lidar particle extinction (dE/dz) and particle number concentration (dN/dz) are adopted to identify the mixed layer depth (MLD) and residual layer depth (RLD).

To obtain a general picture of the diurnal PBL evolution, particle extinction values at different heights in the lower troposphere (0–3 km) were averaged for different time intervals on all sunny days during the campaign. The average vertical profiles in half-hour and 2 h intervals are displayed in Figs. 2 and 3, respectively. The zero and negative values in the lidar measurements were excluded, which may lead to averages slightly overestimated. Averages with less than 75 % data availability were rejected to avoid the impact of undersampling on the average vertical profiles. As mentioned in Sect. 1, the PBL experiences a diurnal cycle. The mixed layer develops after sunrise. Its top rises continually up and may exceed the top of the residual layer formed on the previous day. After the sunset, the mixed layer collapses gradually, forming the nocturnal stable layer and residual layer.

Figures 2 and 3 clearly show the average PBL diurnal cycle of vertical distribution of particle extinction. According to the solar elevation angles, the sunrise and sunset time is estimated to be 05:00–06:00 and 19:00–20:00 LT, respectively. In Fig. 3, the maximum of particle extinction was 0.53 km^{-1} at 660 m after sunset and the top of residual layer was about 705 m. Moreover, the nocturnal stable layer started forming, reaching a depth of about 300 m at 00:00–01:00 LT on the next day (Fig. 3a). During the night, the top of average residual layer fluctuated slightly around 700 m. After sunrise on the next day, the nocturnal stable layer disappeared gradually, and the mixed layer developed. The top of mixed layer reached about 840 m at around 11:00 LT and stayed until 13:00 LT, when it started declining. The particle extinction in the mixed layer increased during the morning period, presumably because of the increasing aerosol emissions, downward mixing from the residual layer, and photochemical production from precursor gases.

The data shown in Figs. 2 and 3 are consistent with our understanding of the diurnal PBL evolution, suggesting that lidar data captured the structure of PBL and can be used in

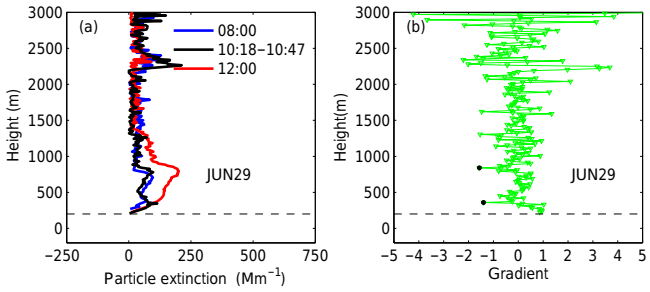

Figure 4. The vertical profile of particle extinction observed during the flight in the late morning of 29 June **(a)** and its gradient **(b)** and the vertical profiles of particle extinction before (blue) and after (red) the flight. The dashed lines indicate the lower limit of lidar.

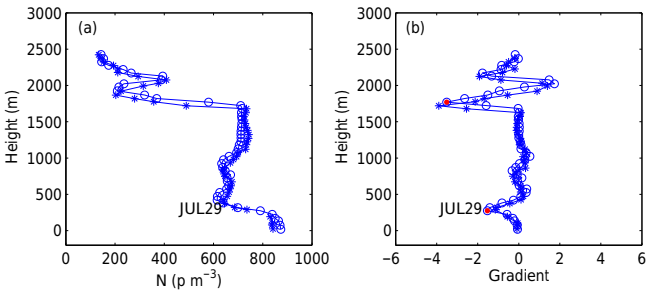

Figure 5. Vertical profiles of aerosol number concentration **(a)** and their gradients **(b)** from the ascent (open circles) and descent (asterisks) flight in the early morning of 29 July (flight 4). The red solid circles indicate the tops of the mixed layer and the residual layer.

the determination of the MLD and RLD. Based on individual dE/dz vertical profiles of particle extinction, we can determine the tops of the mixed layer and residual layer for the periods with UAV flights by identifying the minima below 2000 m in the dE/dz vertical profiles if there were no obviously unreasonable values in the vertical profiles due to interferences or noise. In order to select the minima that were really resulted from a strong decrease of aerosol burden for a small height change rather than abnormal variation, we compared the minima before and after the flights with those during the flights. Finally, the MLD and RLD were obtained according to the heights at which the minima were considered to be the most reasonable ones. However, this method was not applicable when the MLD was in the blind zone of lidar (lower than 200 m) or when there was cloud near the top of residual layer.

The vertical profile of particle extinction and its gradient for the flight (10:18–10:47 LT) in the late morning of 29 June (flight 1) are displayed in Fig. 4 to show how to determine the MLD and RLD. To facilitate the identification of the mixed layer and residual layer, the vertical profiles of particle extinction before and after the flight are also shown in Fig. 4a. With the consideration of turbulent timescale in the atmosphere, the particle extinction vertical profiles at 08:00 and 12:00 LT were calculated from the lidar observations in the periods 07:30–08:30 and 11:30–12:30 LT, respectively. As can be seen in Fig. 4b, there are a few minima in the calculated gradient, two of which (marked with filled black circles) may represent the tops of the mixed layer and residual layer. Comparing the vertical profile of particle extinction during the flight with those before and after the flight, we can see gradual changes in heights of the inflection points in the lower parts of the vertical profiles (0–1500 m) with the evolution of the PBL. This makes us more certain that the filled black circles in the gradient curve in Fig. 4b indicate the tops of the mixed layer and residual layer.

Similar to the vertical gradient of particle extinction, the vertical gradient of aerosol number concentration can also be used to probe the PBL. To find out the key inflection points in the vertical profiles, which indicate the tops of the mixed layer and residual layer, we paid attention to the major structures in vertical profiles and gradients of aerosol number concentration during the ascent and descent flights. Due to the slight differences in time and space in the flight, there were some differences in particle number concentrations measured at the same height between the ascent and descent of a flight. Even though, the t test ($\alpha = 0.05$) may help to judge whether or not the results are accordant. As an example, Fig. 5 shows the aerosol number concentration data from a flight in the early morning of 29 July (flight 4). The two minima at 275 and 1770 m (marked with red solid circles) in the gradient curve (Fig. 5b) obviously corresponds to the major inflection points in the vertical profile of ascent flight (Fig. 5a). In the gradient curve from the descent flight, there are also two minima below 2000 m. These two minima do not overlay those from the ascent flight, but there are no significant ($\alpha = 0.05$) differences in the minimum positions between ascent and descent. Therefore, the marked heights of 275 and 1770 m are considered to be the tops of the mixed layer and the residual layer, respectively.

Determining the MLD and RLD facilitates the calculations of average O_3 and aerosol number concentrations in the mixed layer and the residual layer. Table 2 summarizes the mixed and residual layer heights, determined using the methods discussed above, and the calculated O_3 and aerosol number concentrations for the two layers during the flights. The MLD or RLD during some flights cannot be determined in the case that the MLD was in the blind zone of lidar (lower than 200 m) or there was cloud near the top of residual layer. Ideally, the mixed and residual layer heights determined using the two methods were the same, so this would be the average O_3 and aerosol number concentrations. However, the real conditions were not idealized. As can be seen in Table 2, the two methods produced different results of the MLD and RLD, and the average O_3 and aerosol number concentrations.

To see how the results from the two methods are different from each other, we conducted correlation analyses. In Fig. 6, average O_3 and aerosol number concentrations obtained us-

Table 2. O_3 and aerosol number concentrations calculated in the method of particle extinction gradient (left of "/") and the method of aerosol number concentration gradient (right of "/"). The O_3 concentration on the surface is obtained in the surface measurement program.

		Early morning			Late morning	Afternoon		
		1 Jul (flight 3) 06:34–07:07	29 Jul (flight 4) 07:35–08:04	31 Jul (flight 5) 05:53–06:33	29 Jun (flight 1) 10:18–10:47	29 Jun (flight 2) 17:58–18:38	31 Jul (flight 6) 17:26–18:02	2 Aug (flight 7) 15:17–15:45
Surface	O_3 (ppb)	20.8 ± 0.7	39.7 ± 0.81	29.6 ± 2.5	73.7 ± 1.7	97.8 ± 0.98	87.1 ± 1.4	84.3 ± 2.58
Mixed layer	Height (m)	: : /200	255/275	255/275	360/281	795/525	795/::	::/765
	O_3 (ppb)	::/37.4 ± 20.8	44.3 ± 8.5/44.3 ± 8.5	70.5 ± 38.6/72.4 ± 38.2	71.2 ± 9.0/69.1 ± 9.6	106.7 ± 7.9/103.2 ± 9.2	99.1 ± 5.4/::	104.2 ± 4.9/::
	N (10^2 p cm^{-3})	::/1.99 ± 0.36	8.7 ± 0.12/8.69 ± 0.13	5.73 ± 2.00/5.73 ± 2.00	4.17 ± 0.75/4.54 ± 0.75	6.28 ± 0.17/6.39 ± 0.10	::/::	::/::
Residual layer	Height (m)	1215/1331	::/1770	1110/1577	840/974	::/::	::/::	::/::
	O_3 (ppb)	103.4 ± 12.4/105.1 ± 8.24	::/111 ± 10.7	97 ± 9.23/99.6 ± 8.9	66.5 ± 6.1/65.8 ± 8.5	::/::	::/::	::/::
	N (10^2 p cm^{-3})	1.17 ± 0.18/1.12 ± 0.16	::/6.77 ± 0.52	5.45 ± 0.48/5.38 ± 0.47	2.57 ± 0.08/2.64 ± 0.25	::/::	::/::	::/::

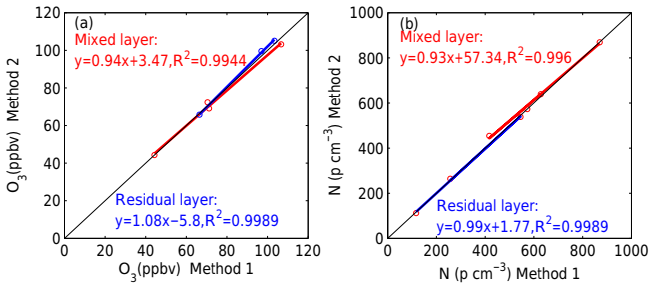

Figure 6. Average O_3 mixing ratios **(a)** and aerosol number concentrations **(b)** in the mixed layer and residual layer obtained using the method of particle extinction gradient (method 1) in comparison with those obtained using the method of particle number concentration gradient (method 2).

ing the method of particle extinction gradient (method 1) are compared with those obtained using the method of particle number concentration gradient (method 2). As can be seen in the figure, the averages obtained using the two methods are highly significantly correlated. Linear regressions suggest that the slopes of correlation lines for average O_3 and aerosol number concentrations in the mixed layer and residual layer are all close to 1.0. In other words, the two methods used for the determination of the MLD and RLD are reliable and can produce comparable results.

3.3 Average O_3 and aerosol number concentrations in the mixed and residual layers

Data in Table 2 indicate that the mixed layer height increased from early morning to late morning and to afternoon. The top of residual layer did not show such tendencies. The mixing ratio of O_3 in the surface layer and mixed layer was the lowest in the early morning and the highest in the afternoon. This can be readily explained by the changes in photochemical production, NO titration, and dry deposition of O_3 in the course of the day. Photochemical reactions often produce much more O_3 around noon than in the other periods, while NO titration and dry deposition remove O_3 more effective during the night and early morning, when the NO level is higher and the mixed layer is shallower (see Fig. S4 in the Supplement). In most cases, the diurnal cycle of surface O_3 can be well explained by these factors, if advection is negligible. However, there may be additional factors that contribute significantly to the diurnal variations of O_3 in the mixed layers, at least in our cases. Table 2 shows that the level of O_3 in the surface and mixed layers were lower than that in the residual layer during all early morning flights (flights 3–5). Data from the flight in late morning of 29 June (flight 1) indicate that the O_3 level in the residual layer was slightly lower than those in the surface and mixed layers. Figure 1c1 shows that O_3 vertical profiles were relatively straight and the O_3 levels in the surface and mixed layers were close to or slightly lower than those at the heights above the mixed

layer. These suggest that during most of our flights the O_3 levels above the top of mixed layer were higher than those below. Similar vertical O_3 profiles were also observed over a site in Beijing by Ma et al. (2011).

The positive gradient in vertical distribution of O_3 makes the residual layer an important source of O_3 in the mixed layer, particularly during the morning when the top of mixed layer is rapidly elevated. Therefore, downward mixing of O_3 in the residual layer over our site may play an important role in the diurnal cycle of O_3 at ground level and in the mixed layer. Previous studies show that O_3 in the free troposphere over the NCP can be rapidly downward transported to the surface layer, driven by high wind speed in winter (Lin et al., 2011; H. L. Zhang et al., 2014) or nighttime convection processes in summer (Jia et al., 2015). Our data show that even under normal meteorological conditions in summer, downward mixing of O_3 at higher altitudes over the NCP can be a significant contributor to the O_3 level in the mixed layer. The physical processes that influence surface O_3 are normally considered in modern air quality models. It is of interest to test how well the models can simulate the impacts of these processes on surface O_3. Our measurements provide valuable experimental data for validating model results and satellite retrievals, which is outside the scope of this paper.

In contrast to the O_3 level, aerosol number concentration in early morning was higher in the mixed layer than in the residual layer. This can be attributed to the fact that the major sources of primary and secondary aerosols are in the mixed layer. With the PBL development during the daytime, aerosol particles are mixed within a deeper layer as can be seen in Fig. 2.

3.4 Aerosol number-size distributions in the mixed layer and residual layer

The mass concentration, size distribution, and chemical composition of aerosol are closely related to emissions, atmospheric chemistry, and meteorological conditions. The formation of the mixed layer and residual layer reduces the vertical mixing and may cause some differences in the physicochemical properties of aerosols between both layers. Here, we investigate the difference in aerosol number-size distribution between the mixed and residual layers, taking advantage of clear separation of both layers. Aerosol number concentrations in different size bins were averaged for the mixed and the residual layers determined using aerosol number concentration gradients. Figure 7 shows the aerosol number and volume size distributions in the mixed layer and residual layer during early morning of 1 July (flight 3), early morning of 29 July (flight 4), late morning of 29 June (flight 1), and afternoon of 29 June (flight 2). The aerosol volume concentrations were calculated from the measured number-size distributions under the assumption that all particles were spherical.

Obviously, the particle number concentration in the mixed layer was higher than that in the residual layer. This is expected as the mixed layer is normally more impacted by emission sources, which are mainly within the mixed layer. On the other hand, the differences of aerosol number and volume concentration between the mixed layer and the residual layer were more significant in the size range $> 2\,\mu m$ in comparison with the other size ranges. This can be well explained by the fact that the mixed layer is much more influenced than the residual layer by the ground-level emission of aerosol in coarse mode. Moreover, aerosol particles were overwhelmingly distributed in the size range $< 1\,\mu m$, independent of observation time. Such aerosol size distribution and ranges of aerosol number concentrations unsurprisingly resembled urban aerosol (Baron et al., 2011). Although some coarse particles may be released by the farm over which our UAV observations were conducted, their contribution to our measurements of aerosol number concentration should be limited within the surface layer, considering the wind conditions during the UAV flights. In other word, the aerosol size distributions at higher altitudes of the PBL were not substan-

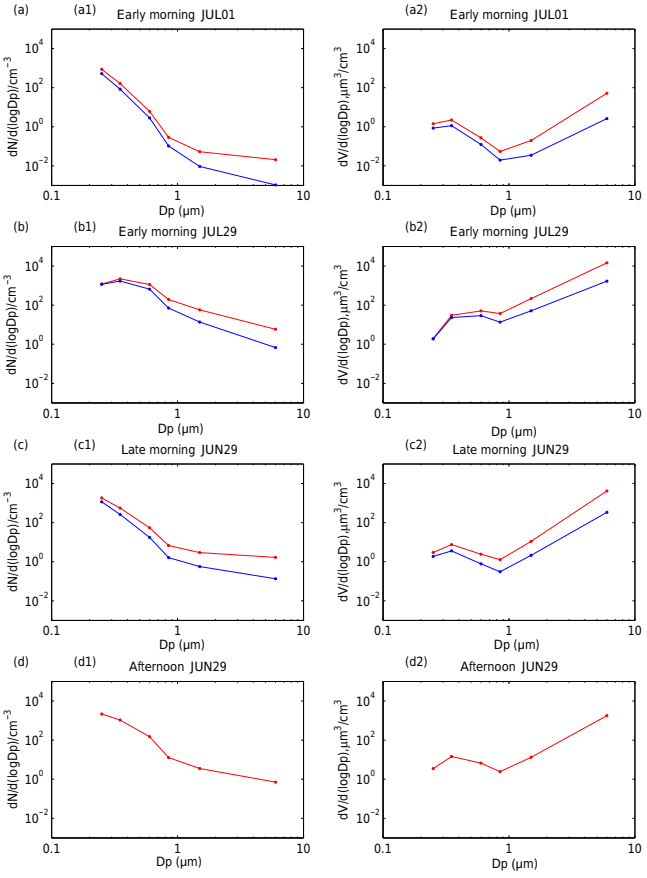

Figure 7. Aerosol number and volume size distributions in the mixed layer (red) and residual layer (blue), in the early morning of 1 July **(a)** and 29 July **(b)**, late morning of 29 June **(c)**, and afternoon of 29 June **(d)** flights. The mixed layer and residual layer heights are determined using the method of aerosol number concentration gradient.

tially influenced by local coarse-particle emissions. In recent decades, the NCP region has been found to be one of the most polluted regions of the world, suffering severe haze pollution (Fu et al., 2014). Even in the rural areas of the NCP, air quality is largely impacted by anthropogenic pollutants locally emitted or transported from urban areas (Lin et al., 2008, 2009; Liu et al., 2010). Therefore, aerosol size distributions shown in Fig. 7 should represent well-mixed aerosol over a rural area in the NCP, which is dominated by fine particles.

It is interesting to see that the patterns of aerosol number and volume size distributions in flight 4 (early morning in 29 July) are different from those in flights 1 (late morning in 29 June), 2 (afternoon in 29 June), and 3 (early morning in 1 July). The number-size distributions in flights 1, 2, and 3 show monotonic decreasing with increasing aerosol size (Fig. 7a, c, and d), while those in flight 4 peak in the range of 0.3–0.5 µm (Fig. 7b). The aerosol size distribution in the early morning of 29 July (flight 4) was unique in that a larger portion of aerosol particles was found in the range 0.3–0.5 µm. It may be caused by different synoptic conditions. Figure 1 indicates that among all the vertical profiles, the vertical profiles from 1 July (flight 3) and 29 July (flight 4) represent most clean and most polluted cases, respectively. Backward trajectories (Fig. S3 in the Supplement) indicate that in early morning of 29 July, air masses were from the southeast sector. Studies at other NCP sites also show that air masses from the southeast are associated with higher particle number concentration (Shen et al., 2011) and contain aerosols of relatively larger mean medium diameter (Y. M. Zhang et al., 2014), which coincide with our results.

3.5 Comparison with historic O_3 vertical profiles

The increase in emissions of air pollutants in the NCP region has caused haze and O_3 pollution in recent decades. Emission control measures that have been introduced in this region have led to a decreasing trend after 2003 in the annual number of haze days (Fu et al., 2014). However, the O_3 air quality has not been improved yet. In contrast, the maximum daily average 8 h (MDA8) mixing ratios of O_3 at a background site in the NCP increased at a rate of 1.13 ppb year^{-1} from 2003 to 2015 (Ma et al., 2016). The increase of O_3 levels has taken place not only at ground level but also at other altitudes in the troposphere, particularly in the PBL. Ding et al. (2008) revealed a strong positive trend of the O_3 level in the boundary layer over Beijing from 1995 to 2005 using the Measurements of Ozone and Water Vapor by Airbus In-Service Aircraft (MOZAIC). Multi-year ozonesonde measurements over Beijing also indicate a significant increase of tropospheric O_3 during the period 2002–2010 (Wang et al., 2012).

It is of great interest to see how lower-tropospheric O_3 has changed over the NCP region. Many locations in the NCP region are controlled by similar prevailing winds (southwesterly and northeasterly), particularly in summer (Lin et al., 2008, 2009). Although the MOZAIC measurements and our UAV observations of O_3 were conducted over two sites about 200 km apart from each other, O_3 vertical profiles in the lower troposphere over both sites may represent the situations over the northern part of the NCP. Therefore, it is assumed that the O_3 vertical profiles over both sites might be comparable. Under this assumption, we can try to obtain an idea about the change of summer O_3 in the lower troposphere over the NCP between the first MOZAIC measurements and our measurements.

Figure 8 displays average O_3 vertical profiles for different time periods of the day in the lower troposphere obtained at the RMS during our tethered balloon (Fig. 8a) and UAV observations (Fig. 8b), and summer daytime (05:00–19:00 LT) average O_3 vertical profiles from MOZAIC observations and our observations (Fig. 8c). The MOZAIC O_3 data have an estimated accuracy of $\pm[2\,\text{ppb} + 2\,\%]$ for individual 4 s measurements and is suitable for building reliable O_3 climatologies (Thouret et al., 1998; Zbinden et al., 2013). MOZAIC O_3 vertical profile data for the greater Beijing area are available only for 1994–2005 with varying monthly vertical profile numbers and most of the vertical profiles were obtained during 05:00–18:00 LT period (Ding et al., 2008). To enhance the representativeness of average vertical profiles, all average MOZAIC O_3 vertical profiles were calculated from at least seven individual vertical profiles. For some years, no average MOZAIC O_3 vertical profiles were available due to inadequate MOZAIC measurements in summer. O_3 measurements from 52 tethered balloon experiments) over Raoyang were grouped and averaged for the early morning (05:00–10:00 LT), late morning (10:00–12:00 LT), and afternoon (12:00–19:00 LT) periods (Fig. 8a). Only seven UAV experiments could be made during our campaign at Raoyang. Nevertheless, average O_3 vertical profiles were calculated for early morning, late morning, and afternoon (Fig. 8b). It is noted that only one UAV flight was made in late morning (flight 1; 10:28–10:50 LT on 29 June 2014); therefore, the late morning average O_3 vertical profile in Fig. 8b is less representative. If this vertical profile is not considered, we can see in Fig. 8a and b a clear development of vertical O_3 distribution in the lower troposphere, with a substantial increase of the O_3 level in the mixed layer and a slight increase above the mixed layer in the course of the early morning to the afternoon. Although the mixing ratios of O_3 over Raoyang were mostly higher than 100 ppb in the afternoon, the overall average values were about 100 ppb as shown in the bottom-right plot of Fig. 8c. Both our measurements and the MOZAIC measurements indicate high-O_3 pollution in the lower troposphere over the NCP in summer.

Figure 8c shows that the O_3 level over the NCP had experienced a strong positive increase, indicating strengthening photochemical pollution in about 2 decades. The average mixing ratio of O_3 near the ground level had a relatively small increase (8.9 ppb) during 2004–2014, corresponding to

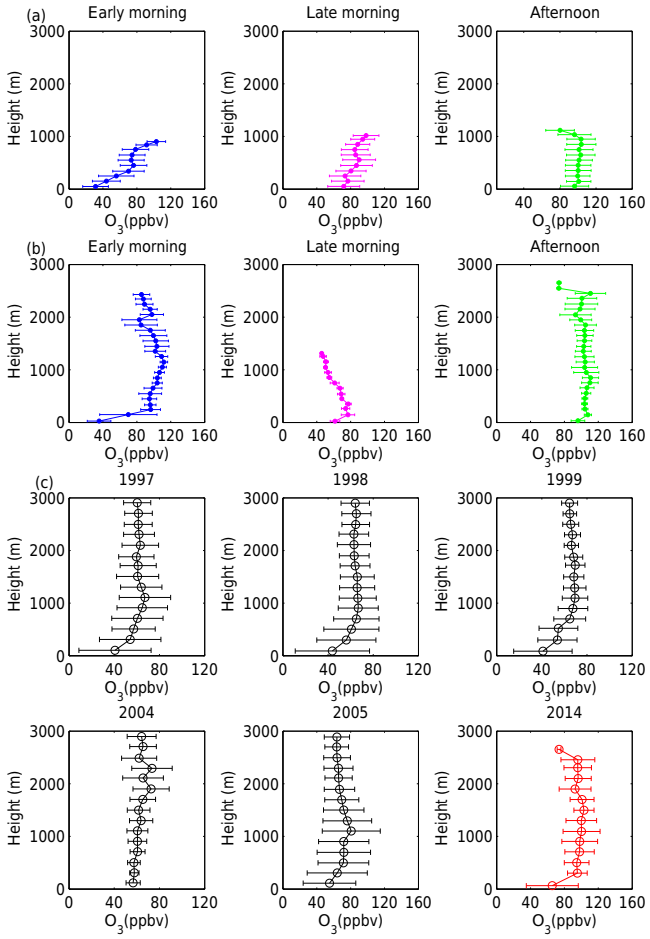

Figure 8. Comparison of average O_3 vertical profiles observed in the lower troposphere during summer of different years. **(a)** shows O_3 vertical profiles from the tethered balloon experiments during summer of 2014 averaged over early morning (05:00–08:00 LT), late morning (08:00–12:00 LT), and afternoon (12:00–19:00 LT). Panel **(b)** presents O_3 vertical profiles from the UAV experiments during summer of 2014 averaged over early morning (flights 3, 4, and 5), late morning (flight 1), and afternoon (flights 2, 6, and 7). Panel **(c)** shows O_3 vertical profiles averaged over daytime (05:00–19:00 LT) MOZAIC measurements in summer of 1997, 1998, 1999, 2004, 2005, and our Raoyang measurement in summer of 2014. The error bars indicate 1 standard error of the mean.

an increase rate of about 0.9 ppb year^{-1}. This increase rate is close to the average increase rate (1.1 ppb year^{-1}) reported by Tang et al. (2009) of surface O_3 at six urban/suburban sites in Beijing in July–September during 2001–2006, but only about one-third of what Q. Zhang et al. (2014) found for August daytime surface O_3 at an urban site in Beijing during 2005–2011 (2.6 ppb year^{-1}). However, the high-end value of O_3 near the ground level had a larger increase, as suggested by the right end of the error bars (Fig. 8c). This larger increase in the high-end value of O_3 is consistent with the large increase of the maximum daily average 8 h (MDA8) mixing ratio of O_3 at the Shangdianzi background station (Ma et al., 2016). Compared with the increase of O_3 near the ground level, much larger increases were found in O_3 at higher altitudes in the lower troposphere over Raoyang during 2004–2014, with the maximum increase (41.6 ± 15.5 ppb) being found at 1.5 km. Assuming that the O_3 level increased linearly over the 10 years, the increase rate would be about 4.2 ± 1.6 ppb year^{-1}. Sun et al. (2016) compiled and analyzed the O_3, NO_x, and CO data collected at the Mt. Tai site (36.25° N, 117.10° E; 1534 m a.s.l.) during a few campaigns from 2003 to 2015. They reported that O_3 at Mt. Tai increased at 1.7 ± 1.0 ppb year^{-1} in June and 2.1 ± 0.9 ppb year^{-1} in July–August during 2003–2015. These rates of increase in summer O_3 at Mt. Tai and that we obtained for 1.5 km over Raoyang agree within the uncertainties though both sites are about 240 km apart. Based on the MOZAIC measurements over Beijing in summer afternoons (at 15:00–16:00 LT in May–June–July), during 1995–2005, Ding et al. (2008) reported an increase rate of about 3 ppb year^{-1} for O_3 in 0–2 km. From the data shown in Fig. 8c, we can obtain an increase rate of 3.3 ppb year^{-1} for summer O_3 in 0–2 km over Raoyang for the period 2004–2014, which agrees well with that reported by Ding et al. (2008). Note that the average O_3 vertical profile for summer 2014 (Fig. 8c) contains measurements from the morning flights so that our estimated increase rate may be significantly lower than that for summer afternoon.

The above comparisons confirm that the abundance of O_3 in the lower troposphere over the northern part of the NCP has largely increased for ca. 2 decades. The increase of the O_3 level in summer afternoon period seems to speed up after 2004. Network observations indicate that surface O_3 pollution in China's polluted regions, including the NCP, has become more severe in recent years in contrast with the apparent decreases of $PM_{2.5}$ and primary gaseous pollutants (http://www.cnemc.cn/publish/totalWebSite/0492/newList_1.html). Such a trend in surface O_3 may exert significant impacts on human health and vegetation. The increase of O_3 in the lower troposphere may influence atmospheric chemistry, i.e., increase the oxidation capacity (Ma et al., 2012) and add radiation forcing over the region.

4 Conclusion

In this study, vertical profiles of particle extinction property, O_3, and size-resolved aerosol concentration were simultaneously measured using miniature devices installed in an UAV over a rural site in the NCP during the summer of 2014, allowing for the characterization of diurnal O_3 and aerosol concentration in mixing layer and residual layer over a small area. Seven vertical profiles were successfully obtained in this campaign.

We found a positive gradient in the vertical distribution of O_3, higher above the top of mixed layer than those be-

low, making the residual layer an important source of O_3 in the mixed layer, particularly during the morning when the top of mixed layer is rapidly elevated. However, aerosol number concentration in the early morning was higher in the mixed layer than in the residual layer. The aerosol particles were abundant and overwhelmingly distributed in the size range < 1 μm, consistent with urban aerosol. The historic O_3 data from the MOZAIC project, together with our measurements, were used to investigate the long-term changes in O_3 vertical profiles in the lower troposphere over the NCP. The comparison of data from the 2014 summer campaign with those from MOZAIC suggests that the O_3 level over the northern part of the NCP has experienced a strong positive increase, and the increase of the O_3 level seems to speed up after 2004, indicating rapidly strengthening photochemical pollution particularly in the last decade. Observations show that surface O_3 pollution in China's polluted regions, including the NCP, has become more severe in recent years in contrast with the apparent decreases of $PM_{2.5}$ and primary gaseous pollutants. In view of this, more attention should be paid to O_3 concentration under the control of PM.

Data availability. The entire data set can be made available for scientific purposes upon request to the corresponding author.

The Supplement related to this article is available online at doi:10.5194/acp-17-3891-2017-supplement.

Competing interests. The authors declare that they have no conflict of interest.

Acknowledgements. This research was supported by the National Natural Science Foundation of China (no. 41330442) and China Special Fund for Meteorological Research in the Public Interest (no. GYHY201206015). We thank Zhiping Liu, Min Sun, and Chaohui Wu for their assistance in the UAV observations, and Yong Wang, Chuncheng Ji, Qihua Du, Hanze Yu, and Xinpan Li for their assistance in the tethered balloon observations. Logistic support from the Raoyang Meteorological Bureau is highly appreciated. The authors acknowledge the strong support of the European Commission, Airbus, and the Airlines (Lufthansa, Air France, Austrian, Air Namibia, Cathay Pacific, Iberia, and China Airlines, so far), who carry the MOZAIC or IAGOS equipment and have performed the maintenance since 1994. In its last 10 years of operation, MOZAIC has been funded by INSU-CNRS (France), Météo-France, Université Paul Sabatier (Toulouse, France), and Research Center Jülich (FZJ, Jülich, Germany). IAGOS has been additionally funded by the EU projects IAGOS-DS and IAGOS-ERI. The MOZAIC-IAGOS database is supported by AERIS (CNES and INSU-CNRS). Data are also available via AERIS website http://aeris-data.fr.

Edited by: A. B. Guenther
Reviewed by: two anonymous referees

References

Ahrens, C. D.: Essentials of Meteorology: An invitation to the atmosphere, 6th Edn., Cengage Learning, 528 pp., 2011.

Altstädter, B., Platis, A., Wehner, B., Scholtz, A., Wildmann, N., Hermann, M., Käthner, R., Baars, H., Bange, J., and Lampert, A.: ALADINA – an unmanned research aircraft for observing vertical and horizontal distributions of ultrafine particles within the atmospheric boundary layer, Atmos. Meas. Tech., 8, 1627–1639, doi:10.5194/amt-8-1627-2015, 2015.

Aneja, V. P., Mathur, R., Arya, S. P., Li, Y., Murray, G. C., and Manuszak, T. L.: Coupling the vertical distribution of ozone in the atmospheric boundary layer, Environ. Sci. Technol., 34, 2324–2329, 2000.

Anenberg, S. C., West, J. J., Fiore, A. M., Jaffe, D. A., Prather, M. J., Bergmann, D., and Hess, P.: Intercontinental impacts of ozone pollution on human mortality, Environ. Sci. Technol., 43, 6482–6487, 2009.

Baron, P. A., Kulmarni, P., and Willeke, K. (Eds.): Aerosol Measurement: principles, techniques, and applications, 3rd Edn., John Wiley & Sons, Inc. Publication, New Jersey, USA, 2011.

Brooks, I. M.: Finding boundary layer top: Application of a wavelet covariance transform to lidar backscatter profiles, J. Atmos. Ocean. Tech., 20, 1092–1105, 2003.

Charlson, R. J.: Direct climate forcing by anthropogenic sulfate aerosols: The Arrhenius paradigm a century later, Ambio, 26, 25–31, 1997.

Chen, P. F., Zhang, Q., Quan, J. N., Gao, Y., Zhao, D. L., and Meng, J.: Ground-high altitude joint detection of ozone and nitrogen oxides in urban areas of Beijing, J. Environ. Sci., 25, 758–769, 2013.

Chen, X., Huang, F., Xia, X., Cao, J., and Xu, X.: Analysis of tropospheric ozone long-term changing trends and affecting factors over northern China, Chinese Sci. Bull., 60, 2659–2666, doi:10.1360/N972015-00155, 2015 (in Chinese with English abstract).

Chen, Y., Zhao, C., Zhang, Q., Deng, Z., Huang, M., and Ma, X.: Aircraft study of Mountain Chimney Effect of Beijing, China, J. Geophys. Res., 114, D08306, doi:10.1029/2008JD010610, 2009.

Cohn, S. A., Grund, C. J., Mayor, S. D., and Angevine, W. M.: Boundary layer height and vertical velocity measurements at LIFT, 12th Symp. on Boundary Layers and Turbulence, Vancouver, BC, Canada, Am. Meteorol. Soc., 7–8, 1997.

Coakley Jr., J. A., Cess, R. D., and Yurevich, F. B.: The effect of tropospheric aerosols on the Earth's radiationbudget: A parameterization for climate models, J. Atmos. Sci., 40, 116–138, 1983.

Ding, A. J., Wang, T., Thouret, V., Cammas, J.-P., and Nédélec, P.: Tropospheric ozone climatology over Beijing: analysis of aircraft data from the MOZAIC program, Atmos. Chem. Phys., 8, 1–13, doi:10.5194/acp-8-1-2008, 2008.

Ding, Y. H. and Liu, Y. J.: Analysis of long-term variations of fog and haze in China in recent 50 years and their relations with atmospheric humidity, Science China: Earth Sciences, 57, 36–46, doi:10.1007/s11430-013-4792-1, 2014.

Draxler, R. R. and Rolph, G. D.: HYSPLIT (HYbrid SingleParticle Lagrangian Integrated Trajectory), Model access via NOAA ARL READY, available at: http://www.arl.noaa.gov/ready/hysplit4.html (last access: 18 March 2017), NOAA Air Resources Laboratory, Silver Spring, MD, 2003.

Fast, J. D. and Berkowitz, C. M.: A modeling study of boundary layer processes associated with ozone layers observed during the 1993 North Atlantic Regional Experiment, J. Geophys. Res., 101, 28683–28699, 1996.

Feng, Z., Kobayashi, K., and Ainsworth, E. A.: Impact of elevated ozone concentration on growth, physiology, and yield of wheat (*Triticum aestivum* L.): a meta-analysis, Glob. Change Biol., 14, 2696–2708, 2008.

Ferrero, L., Riccio, A., Perrone, M. G., Sangiorgi, G., Ferrini, B. S., and Bolzacchini, E.: Mixing height determination by tethered balloon-based particle soundings and modeling simulations, Atmos. Res., 102, 145–156, 2011.

Ferrero, L., Castelli, M., Ferrini, B. S., Moscatelli, M., Perrone, M. G., Sangiorgi, G., D'Angelo, L., Rovelli, G., Moroni, B., Scardazza, F., Mocnik, G., Bolzacchini, E., Petitta, M., and Cappelletti, D.: Impact of black carbon aerosol over Italian basin valleys: high-resolution measurements along vertical profiles, radiative forcing and heating rate, Atmos. Chem. Phys., 14, 9641–9664, doi:10.5194/acp-14-9641-2014, 2014.

Fu, G. Q., Xu, W. Y., Yang, R. F., Li, J. B., and Zhao, C. S.: The distribution and trends of fog and haze in the North China Plain over the past 30 years, Atmos. Chem. Phys., 14, 11949–11958, doi:10.5194/acp-14-11949-2014, 2014.

Gao, R. S., Telg, H., McLaughlin, R. J., Ciciora, S. J., Watts, L. A., Richardson, M. S., Schwarz, J. P., Perring, A. E., Thornberry, T. D., Rollins, A. W., Markovic, M. Z., Bates, T. S., Johnson, J. E., and Fahey, D. W.: A light-weight, high-sensitivity particle spectrometer for $PM_{2.5}$ aerosol measurements, Aerosol Sci. Tech., 50, 88–99, 2016.

Hayden, K. L., Anlauf, K. G., Hoff, R. M., and Strapp, J. W.: Pacific'93 lower Fraser Valley oxidants study aircraft data report, Environment Canada Report, 268 pp., 1994.

He, Q. S. and Mao, J. T.: Observation of urban mixed layer at Beijing using a micro pulse lidar, Acta Meteorologica Sinica, 63, 374-384, 2005.

Hoff, R. M., Guise-Bagley, L., Staebler, R. M., Wiebe, H. A., Brook, J., Georgi, B., and Düsterdiek, T.: Lidar, nephelometer, and in situ aerosol experiments in southern Ontario, J. Geophys. Res., 101, 19199–19209, 1996.

Huang, C. H., Song, X. Q., Wang, G. L., and Lou, Z. S.: Data processing of atmospheric boundary height detected by laser radar during 2009 summer in Zhuhai, Journal of Atmospheric and Environmental Optics, 6, 409–414, 2011.

Illingworth, S., Allen, G., Percival, C., Hollingsworth, P., Gallagher, M., Ricketts, H., and Roberts, G.: Measurement of boundary layer ozone concentrations on-board a Skywalker unmanned aerial vehicle, Atmos. Sci. Lett., 15, 252–258, 2014.

Jia, S., Xu, X, Lin, W, Wang, Y., He, X., and Zhang, H.: Increased mixing ratio of surface ozone by nighttime convection process over the North China Plain, J. Appl. Meteorol. Sci., 26, 280–290, 2015 (in Chinese with English abstract).

Kiehl, J. T. and Briegleb, B. P.: The relative roles of sulfate aerosols and greenhouse gases in climate forcing, Science, 260, 311–314, 1993.

Kleinman, L., Lee, Y. N., Springston, S. R., Nunnermacker, L., Zhou, X., Brown, R., and Newman, L.: Ozone formation at a rural site in the southeastern United States, J. Geophys. Res., 99, 3469–3482, 1994.

Lenschow, D. H.: Aircraft measurements in the boundary layer, in: Probing the atmospheric boundary layer, edited by: Lenschow, D. H., Am. Meteorol. Soc., 39–55, 1986.

Lin, C. H., Lai, C. H., Wu, Y. L., Lai, H. C., and Lin, P. H.: Vertical ozone distributions observed using tethered ozonesondes in a coastal industrial city, Kaohsiung, in southern Taiwan, Environ. Monit. Assess., 127, 253–270, 2007.

Lin, W., Xu, X., Zhang, X., and Tang, J.: Contributions of pollutants from North China Plain to surface ozone at the Shangdianzi GAW Station, Atmos. Chem. Phys., 8, 5889–5898, doi:10.5194/acp-8-5889-2008, 2008.

Lin, W., Xu, X., Ge, B. Z., and Zhang, X. C.: Characteristics of gaseous pollutants at Gucheng, a rural site southwest of Beijing, J. Geophys. Res., 114, D00G14, doi:10.1029/2008JD010339, 2009.

Lin, W., Xu, X., Ge, B., and Liu, X.: Gaseous pollutants in Beijing urban area during the heating period 2007–2008: variability, sources, meteorological, and chemical impacts, Atmos. Chem. Phys., 11, 8157–8170, doi:10.5194/acp-11-8157-2011, 2011.

Liu, X., Xu, X., and Lin, W.: Variation characteristics of surface O_3 in Beijing and its surrounding area, China Environmental Science, 30, 946–953, 2010.

Ma, J. Z., Wang, W., Chen, Y., Liu, H. J., Yan, P., Ding, G. A., Wang, M. L., Sun, J., and Lelieveld, J.: The IPAC-NC field campaign: a pollution and oxidization pool in the lower atmosphere over Huabei, China, Atmos. Chem. Phys., 12, 3883–3908, doi:10.5194/acp-12-3883-2012, 2012.

Ma, Z., Xu, J., Quan, W., Zhang, Z., Lin, W., and Xu, X.: Significant increase of surface ozone at a rural site, north of eastern China, Atmos. Chem. Phys., 16, 3969–3977, doi:10.5194/acp-16-3969-2016, 2016.

Ma, Z. Q., Zhang, X. L., Xu, J., Zhao, X. J., and Meng, W.: Characteristics of ozone vertical profile observed in the boundary layer around Beijing in autumn, J. Environ. Sci., 23, 1316–1324, 2011.

McKee, D. J.: Tropospheric Ozone: Human Health and Agricultural Impacts, CRC Press, Boca Raton, Florida, USA, 1994.

Melfi, S. H., Spinhirne, J. D., Chou, S. H., and Palm, S. P.: Lidar observations of vertically organized convection in the planetary boundary layer over the ocean, J. Clim. Appl. Meteorol., 24, 806–821, 1985.

Myhre, G., Shindell, D., Bréon, F.-M., Collins, W., Fuglestvedt, J., Huang, J., Koch, D., Lamarque, J.-F., Lee, D., Mendoza, B., Nakajima, T., Robock, A., Stephens, G., Takemura, T., and Zhang, H.: Anthropogenic and Natural Radiative Forcing, in: Climate Change 2013: The Physical Science Basis. Contribution of Working Group I to the Fifth Assessment Report of the Intergovernmental Panel on Climate Change, edited by: Stocker, T. F., Qin, D., Plattner, G.-K., Tignor, M., Allen, S. K., Boschung, J., Nauels, A., Xia, Y.. Bex, V., and Midgley, P. M., Cambridge University Press, Cambridge, UK, New York, NY, USA, 2013.

Neu, U., Künzle, T., and Wanner, H.: On the relation between ozone storage in the residual layer and daily variation in near-surface ozone concentration – A case study, Bound.-Lay. Meteorol., 69, 221–247, 1994.

Ran, L., Deng, Z., Xu, X., Yan, P., Lin, W., Wang, Y., Tian, P., Wang, P., Pan, W., and Lu, D.: Vertical profiles of black carbon measured by a micro-aethalometer in summer in the North China Plain, Atmos. Chem. Phys., 16, 10441–10454, doi:10.5194/acp-16-10441-2016, 2016.

Rauneker, P. and Lischeid, G.: Spatial distribution of water stress and evapotranspiration estimates using an unmanned aerial vehicle (UAV), Geophys. Res. Abstr., EGU2012-10477, EGU General Assembly 2012, Vienna, Austria, 2012.

Schwartz, S. E.: The whitehouse effect – Shortwave radiative forcing of climate by anthropogenic aerosols: An overview, J. Aerosol Sci., 27, 359–382, 1996.

Seinfeld, J. H. and Pandis, S. N.: Atmospheric Chemistry and Physics – From Air Pollution to Climate Change, 2nd Edn., John Wiley and Sons, New Jersey, USA, 2006.

Shen, X. J., Sun, J. Y., Zhang, Y. M., Wehner, B., Nowak, A., Tuch, T., Zhang, X. C., Wang, T. T., Zhou, H. G., Zhang, X. L., Dong, F., Birmili, W., and Wiedensohler, A.: First long-term study of particle number size distributions and new particle formation events of regional aerosol in the North China Plain, Atmos. Chem. Phys., 11, 1565–1580, doi:10.5194/acp-11-1565-2011, 2011.

Steyn, D. G., Baldi, M., and Hoff, R. M.: The detection of mixed layer depth and entrainment zone thickness from lidar backscatter profiles, J. Atmos. Ocean. Tech., 16, 953–959, 1999.

Sun, L., Xue, L., Wang, T., Gao, J., Ding, A., Cooper, O. R., Lin, M., Xu, P., Wang, Z., Wang, X., Wen, L., Zhu, Y., Chen, T., Yang, L., Wang, Y., Chen, J., and Wang, W.: Significant increase of summertime ozone at Mount Tai in Central Eastern China, Atmos. Chem. Phys., 16, 10637–10650, doi:10.5194/acp-16-10637-2016, 2016.

Tang, G., Li, X., Wang, Y., Xin, J., and Ren, X.: Surface ozone trend details and interpretations in Beijing, 2001–2006, Atmos. Chem. Phys., 9, 8813–8823, doi:10.5194/acp-9-8813-2009, 2009.

Tegen, I., Koch, D., Lacis, A. A., and Sato, M.: Trends in tropospheric aerosol loads and corresponding impact on direct radiative forcing between 1950 and 1990: A model study, J. Geophys. Res., 105, 26971–26989, 2000.

Thouret, V., Marenco, A., Logan, J. A., Nédélec, P., and Grouhel, C.: Comparisons of ozone measurements from the MOZAIC airborne program and the ozone sounding network at eight locations, J. Geophys. Res., 103, 25695–25720, 1998.

Wang, Y., Konopka, P., Liu, Y., Chen, H., Müller, R., Plöger, F., Riese, M., Cai, Z., and Lü, D.: Tropospheric ozone trend over Beijing from 2002–2010: ozonesonde measurements and modeling analysis, Atmos. Chem. Phys., 12, 8389–8399, doi:10.5194/acp-12-8389-2012, 2012.

Watai, T., Machida, T., Ishizaki, N., and Inoue, G.: A lightweight observation system for atmospheric carbon dioxide concentration using a small unmanned aerial vehicle, J. Atmos. Ocean. Tech., 23, 700–710, 2006.

Xu, X. and Lin, W.: Trends of tropospheric ozone over China based on the satellite data (1979–2005), Advances in Climate Change Research, 2, 43–48, doi:10.3724/SP.J.1248.2011.00043, 2011.

Yue, X. and Unger, N.: Ozone vegetation damage effects on gross primary productivity in the United States, Atmos. Chem. Phys., 14, 9137–9153, doi:10.5194/acp-14-9137-2014, 2014.

Zbinden, R. M., Thouret, V., Ricaud, P., Carminati, F., Cammas, J.-P., and Nédélec, P.: Climatology of pure tropospheric profiles and column contents of ozone and carbon monoxide using MOZAIC in the mid-northern latitudes (24° N to 50° N) from 1994 to 2009, Atmos. Chem. Phys., 13, 12363–12388, doi:10.5194/acp-13-12363-2013, 2013.

Zhang, H. L., Xu, X. B., Lin, W. L., and Wang, Y.: Wintertime peroxyacetyl nitrate (PAN) in the megacity Beijing: the role of photochemical and meteorological processes, J. Environ. Sci., 26, 83–96, 2014.

Zhang, J. and Rao, S. T.: The role of vertical mixing in the temporal evolution of ground-level ozone concentrations (in Chinese with English abstract), J. Appl. Meteorol., 38, 1674–1691, 1999.

Zhang, Q., Yuan, B., Shao, M., Wang, X., Lu, S., Lu, K., Wang, M., Chen, L., Chang, C.-C., and Liu, S. C.: Variations of ground-level O_3 and its precursors in Beijing in summertime between 2005 and 2011, Atmos. Chem. Phys., 14, 6089–6101, doi:10.5194/acp-14-6089-2014, 2014.

Zhang, Y. M., Zhang, X. Y., Sun, J. Y., Hu, G. Y., Shen, X. J., Wang, Y. Q., Wang, T. T., Wang, D. Z., and Zhao, Y.: Chemical composition and mass size distribution of PM_1 at an elevated site in central east China, Atmos. Chem. Phys., 14, 12237–12249, doi:10.5194/acp-14-12237-2014, 2014.

Zheng, X. D., Ding, G. A., Yu, H. Q., Liu, Y., and Xu, X. D.: Vertical distribution of ozone in the planetary boundary layer at the Ming Tombs, Beijing, Sci. China Ser. D, 48, 55–63, 2005.